AGU ADVANCING EARTH AND SPACE SCIENCES

Geophysical Research Letters

RESEARCH LETTER
10.1029/2024GL109584

The Effect of Nitrogen on the Dihedral Angle Between Fe−Ni Melt and Ringwoodite: Implications for the Nitrogen Deficit in the Bulk Silicate Earth

Kyusei Tsuno[1,2], Damanveer S. Grewal[2,3,4], Virginia Xu[5], Logan Leinbach[1,2], Kurt Leinenweber[2,3], Axel Wittmann[1], and Sang-Heon Shim[2,4]

[1]Eyring Materials Center, Arizona State University, Tempe, AZ, USA, [2]Facility for Open Research in a Compressed Environment (FORCE), Arizona State University, Tempe, AZ, USA, [3]School of Molecular Sciences, Arizona State University, Tempe, AZ, USA, [4]School of Earth and Space Exploration, Arizona State University, Tempe, AZ, USA, [5]School for Engineering of Matter, Transport and Energy, Arizona State University, Tempe, AZ, USA

Key Points:

- Dihedral angles of Fe-Ni-N melt in ringwoodite matrix ranged from 112° to 137°, surpassing the wetting boundary
- Percolation of Fe−Ni−N melt through the solid mantle cannot explain N depletion in the bulk silicate Earth
- Fe−Ni−N alloy can be a hidden N reservoir in the mantle if excess N was present in the Earth's mantle post core-mantle differentiation

Supporting Information:

Supporting Information may be found in the online version of this article.

Correspondence to:

K. Tsuno,
ktsuno@asu.edu

Citation:

Tsuno, K., Grewal, D. S., Xu, V., Leinbach, L., Leinenweber, K., Wittmann, A., & Shim, S.-H. (2024). The effect of nitrogen on the dihedral angle between Fe−Ni melt and ringwoodite: Implications for the nitrogen deficit in the bulk silicate Earth. *Geophysical Research Letters*, *51*, e2024GL109584. https://doi.org/10.1029/2024GL109584

Received 3 APR 2024
Accepted 15 AUG 2024

Abstract Nitrogen (N) is extremely depleted in the bulk silicate Earth (BSE). However, whether the silicate magma ocean was as N-poor as the present-day BSE is unknown. We performed multi-anvil experiments at 20 GPa and 1,673−2,073 K to determine the dihedral angle of Fe−Ni−N alloy melt in ringwoodite matrix to investigate whether percolation of Fe-rich alloy melt in the solid mantle can explain N depletion in the BSE. The dihedral angles ranged from 112° to 137°, surpassing the wetting boundary. Our experiments suggest that N removal from the mantle by percolation of Fe-rich alloy melt to the Earth's core is unlikely. Therefore, besides N loss to space during planetesimal and planetary differentiation, as well as its segregation into the Earth core, the stranded Fe-rich metal in the deep mantle could be a hidden N reservoir, contributing to the anomalous depletion of N in the observable BSE.

Plain Language Summary Understanding how and when the present-day inventory of nitrogen (N) in the bulk silicate Earth (BSE) was established is important to gain insights into Earth's habitability. A key question remains as to why N is strongly depleted in the BSE than carbon and hydrogen. Efficient segregation of N into the metallic core in the final stage of Earth's formation is postulated to be one of the primary causes behind this depletion. However, it is not clear whether the silicate magma ocean (MO) was as depleted in N as the present-day BSE due to the uncertainties in the degree of metal-silicate equilibration during the final stages of Earth's formation. Post-MO crystallization, Fe−Ni alloy precipitated in the reduced mantle owing to the disproportionation of ferrous iron. We used high-pressure experiments to examine whether this Fe−Ni alloy melt can trap the excess N and percolate through the solid mantle to the core. Our experiments show that the percolation of Fe−Ni−N melt is unlikely owing to its dihedral angle in silicate phases being larger than the wetting boundary. Instead, the Fe−Ni−N alloy stranded in the mantle can be a hidden N reservoir and the present-day BSE may not be as N-depleted as predicted.

1. Introduction

Nitrogen (N), along with carbon (C) and hydrogen (H), is a key life-forming element and is essential for supporting life on the Earth's surface. The present-day inventory of N on Earth's surficial reservoirs is controlled by its exchange with the silicate interior over billions of years of Earth's history (Gaillard et al., 2021; Grewal et al., 2020; Zahnle et al., 2007). Therefore, in order to understand the origin of the present-day inventory of N in Earth's surficial reservoirs, it is critical to determine the origin of N in the bulk silicate Earth (BSE = atmosphere + hydrosphere + crust + mantle). Nitrogen is depleted in the observable BSE by ∼2–3 orders of magnitude relative to the primitive building blocks of Earth sampled by chondrites (Halliday, 2013; Marty, 2012). The cause of N depletion in the BSE has been linked to −(a) N loss during planetesimal differentiation (Grewal, 2022; Grewal & Asimow, 2023; Grewal et al., 2022a); (b) Segregation of N into the metallic core of the growing Earth (Dalou et al., 2017; Grewal et al., 2019a, 2021b; Speelmanns et al., 2019; Suer et al., 2023); and (c) Atmospheric loss during Earth's formation (Grewal et al., 2021b; Jackson et al., 2021; Kurokawa et al., 2022). The efficacy of these processes in establishing N-depletion remains debated owing to the complexities involved during the stochastic growth of Earth's over tens of millions of years, namely −(a) Accretion of N from multiple reservoirs in the solar protoplanetary disk via a mix of undifferentiated and differentiated materials (Grewal et al., 2021a; Piani et al., 2020); (b) Efficiency of metal-silicate equilibrium between

the impactor's core and proto-Earth's mantle after impacts (Grewal et al., 2024; Rudge et al., 2010); and (c) Efficiency of atmosphere loss during impacts (Grewal et al., 2024; Schlichting et al., 2015).

Limited efficiency of metal-silicate equilibrium (Deguen et al., 2014; Landeau et al., 2016) and the retention of substantial portion of proto-atmosphere(s) (Genda & Abe, 2003; Kegerreis et al., 2018) during giant impacts at the later stages of Earth's growth suggest that the BSE after the main stage of Earth's accretion may not have been as N-depleted as it is in its present state. Processes after the Earth's formation could also have played a role in establishing the N-depletion in the present-day BSE. One of those processes could be precipitation of excess Fe−Ni alloy melt in the post-magma ocean (MO) crystallization mantle, followed by its percolation to the Earth's core through the solid mantle. However, the feasibility of this process has not explored thus far.

Based on the analysis of rocks derived from lithospheric mantle, oxygen fugacity in the Earth's mantle, buffered by the interaction between ferrous (Fe^{2+}) and ferric iron (Fe^{3+}) in the silicate phases, decreases as a function of depth (Frost & McCammon, 2008; Woodland & Koch, 2003). Fe−Ni alloy can precipitate at >250 km depth owing to the following charge disproportionation reaction (Rohrbach et al., 2007; Rohrbach & Schmidt, 2011):

$$3\,Fe^{2+}_{(silicate)} = 2\,Fe^{3+}_{(silicate)} + Fe_{(alloy)} \quad (1)$$

If the excess N was stored in the silicate mantle after early Earth differentiation (e.g., in trapped melts (Hier-Majumder & Hirschmann, 2017) and mantle minerals (Fukuyama et al., 2023; Rustioni et al., 2024; Yoshioka et al., 2018)), it can combine with the precipitated Fe−Ni alloy to form Fe−Ni−N alloy melt at conditions relevant for the mantle geotherm (Katsura, 2022; Katsura et al., 2010). Nitrogen strongly partitions into metallic Fe rather than silicate minerals (e.g., ringwoodite and bridgmanite; Yoshioka et al., 2018). Since 0.3−0.5 wt% metallic Fe can be present in the deep part of mantle transition zone (MTZ) (e.g., 520−660 km depth (Rohrbach et al., 2007; Rohrbach & Schmidt, 2011);), the presence of ∼50–100 ppm N in the Earth's mantle after Earth's formation (Grewal et al., 2019b; Speelmanns et al., 2019) could result in a few percent of N in the Fe−Ni alloy melt. The Fe−Ni−N alloy melt, depending on its wetting behavior with solid silicate minerals, can mobilize and remove the excess N from the Earth's mantle to its core. Iron nitride inclusions in diamonds attest to the presence of Fe−Ni−N alloy in the deep mantle (Kaminsky & Wirth, 2017; Zedgenizov & Litasov, 2017). Therefore, if the percolation of the Fe−Ni−N alloy melt through the silicate minerals to the core is efficient, it could have removed excess N from the solid mantle to establish the present-day N depletion in the BSE.

In this study, we use high pressure-high temperature experiments to examine the wetting behavior of Fe−Ni−N alloy melt in ringwoodite (a major mineral in the deep MTZ), at pressures and temperatures corresponding to the mantle geotherm. We apply our experimental results to examine the role of Fe−Ni−N alloy melt percolation in solid mantle in establishing the N-depletion in the present-day BSE.

2. Experimental Details

The starting materials were mixtures of Fe, Ni, and iron nitride reagent powders and crushed natural San Carlos olivine. To study the effects of Ni and N content on the dihedral angle, three different alloy compositions were prepared: Ni-free with 1 wt% N, Ni-free with 4 wt% N, and 10 wt% Ni with 4 wt% N (Supplementary Table 1 in Supporting Information S1). Addition of 10 wt% Ni to the starting alloy mixture results in the Ni content in the recovered alloy products being similar to that of metallic alloys in the Earth's MTZ (Supplementary Table 2 in Supporting Information S1) (Frost & McCammon, 2008; Rohrbach & Schmidt, 2011). Addition of 1–4 wt% N in the starting alloy mixture simulates Fe−Ni−N alloys, where 0.3−0.5 wt% alloy precipitated in the deep MTZ (Rohrbach & Schmidt, 2011) and equilibrated with a mantle containing ∼30−500 ppm N. The volume fraction of the alloy mixture in the starting material was 2 vol.%, which is below the critical melt fraction required for forming interconnected network when the dihedral angle is greater than 60° (von Bargen & Waff, 1986).

The high-pressure experiments at 20 GPa and 1,673−2,073 K were carried out using a 1,000 ton Walker-type multi-anvil device at Arizona State University (ASU), following the procedure of Leinenweber et al. (2012). The experimental temperature is in the range of the mantle geotherm in the MTZ (Katsura, 2022; Katsura et al., 2010) and higher than the melting temperature of iron nitride (Kusakabe et al., 2019). Following the procedure of previous studies (Grewal et al., 2021c; Tsuno et al., 2018), the sample was initially heated to and kept overnight at 1,123−1,173 K to reduce the porosity of MgO capsule, and then heated to the target temperature

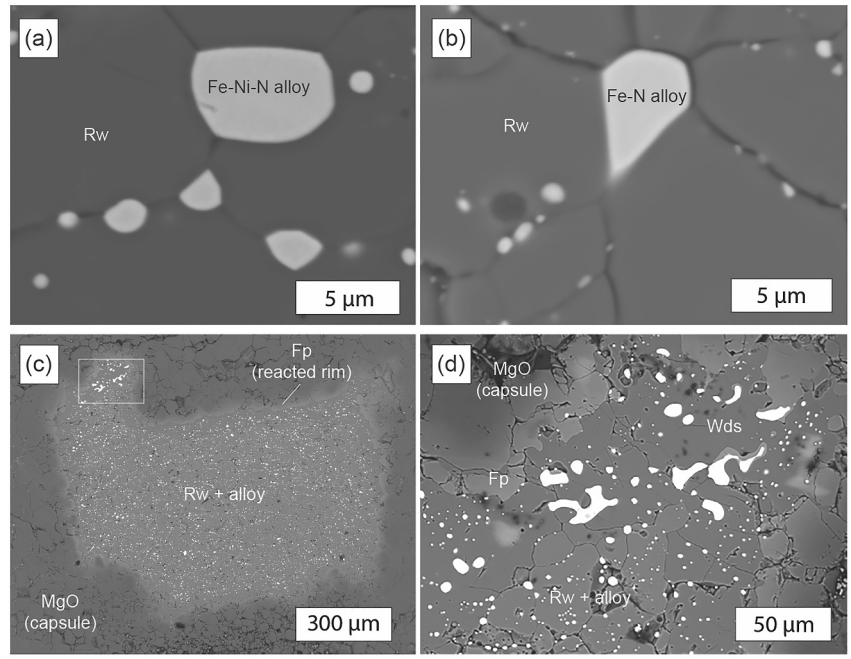

Figure 1. Representative back-scattered electron images of the experimental run products. (a) Experiments at 20 GPa and 1,873 K (BB1644). For most of the run products except for BB1669, the dihedral angle would be distributed in the range of ~80°–160°. (b) Experiments at 20 GPa and 2,073 K (BB1669). The median value of dihedral angle (true dihedral angle, in other words) of this run is the smallest of all of the experimental run charges in our study. In this recovered sample, alloy melts with dihedral angles smaller than 60° were also observed. (c) The overall image of BB1669. It can be seen that most of the sample region was composed of Fe−N alloy melts and ringwoodite. (d) Detail of the experimental run marked in rectangle in (c), showing that small amount of wadsleyite was observed in the sample area close to thermocouple. Also shown are ferropericlase formed by the diffusion of Fe in alloy melt and FeO in ringwoodite and wadsleyite in MgO capsule.

of 1,673 K for 16 hr, of 1,873 K for 6−8 hr, and of 2,073 K for 2 hr. Terasaki et al. (2005) and Shannon & Agee (1996) conducted time-series experiments to demonstrate the attainment of textural equilibrium of Fe (−O)−S alloy melts, achieving relatively constant dihedral angles in 12 hr at 1,650 K and 2.4 hr at 2,033 K, respectively. Given that our experiments were conducted for 16 hr at 1,673 K, 8 hr at 1,873 K, and 2 hr at 2,073 K − durations that are longer or comparable to those in the studies by Terasaki et al. (2005) and Shannon & Agee (1996) − it is expected that our experiments had attained textural equilibrium.

The recovered samples were analyzed using a micro-Raman spectroscopy for phase identification and a JEOL JXA-8530F electron microprobe for chemical and image analysis at 15 kV and 15 nA at ASU. Synthetic iron nitride (Fe_3N) was used as a standard for N in the metallic alloy and it was measured using an LDE2 spectrometer crystal, consistent with Grewal et al. (2019a, 2019b, 2021b).

The apparent dihedral angle was measured using backscattered electron images of the recovered samples (Figure 1). Dihedral angle measurements were performed using the image processing program "Image J." The true dihedral angle of Fe−Ni−N alloy melts in ringwoodite was the median of the apparent dihedral angle distribution (Supplementary Table 1 in Supporting Information S1 and Figure 2). The measurement error of the dihedral angle is based on a 95% confidence interval centered on the population median. Each sample underwent a sufficient number of dihedral angle measurements, ranging from 219 to 258, ensuring accurate determination of the true dihedral angle (Holness & Lewis, 1997).

3. Results

3.1. Texture of the Experimental Products

All the recovered products consisted of quenched Fe(−Ni)−N alloy and ringwoodite (Supplementary Table 1 in Supporting Information S1, Figures 1a and 1b, and Supplementary Figure 1 in Supporting Information S1), except for one sample (Exp. No. BB1669), which contained a small amount of wadsleyite in the sample region close to

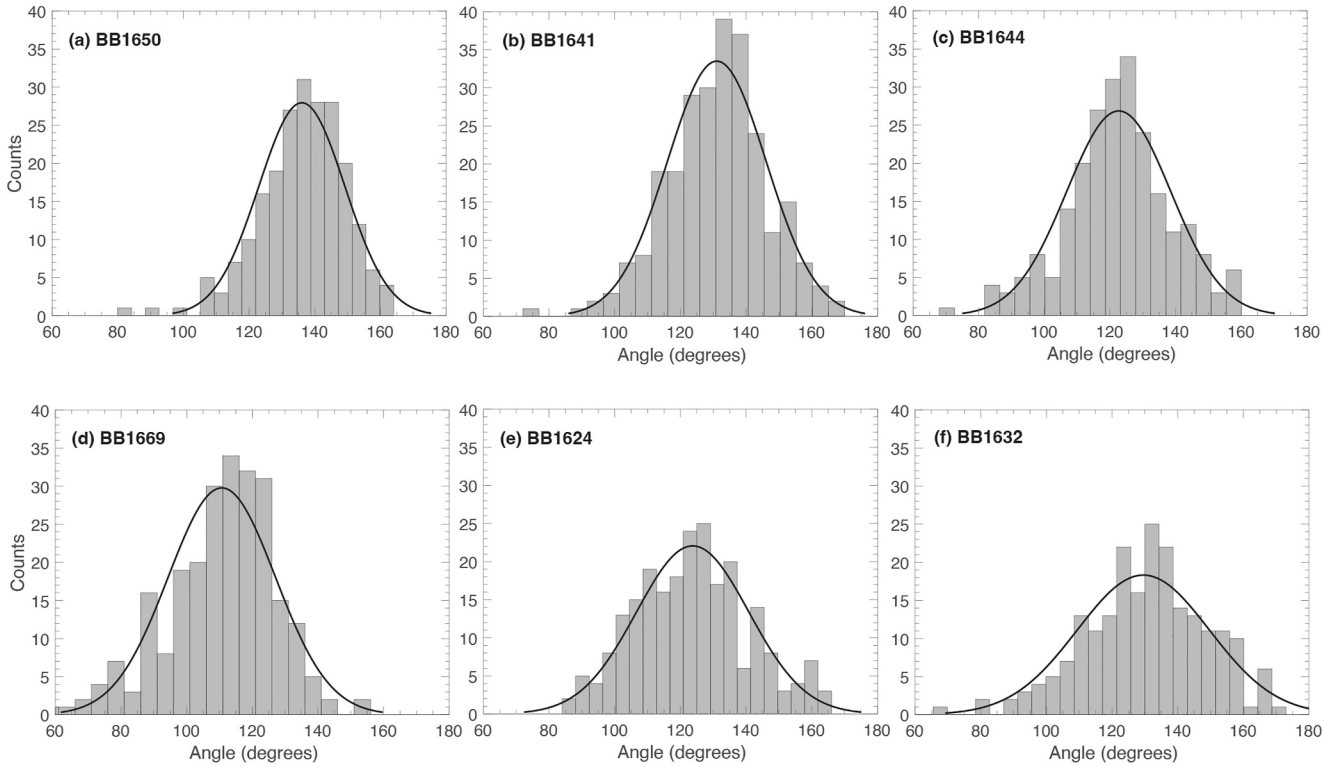

Figure 2. The apparent dihedral angle distribution based on the back-scattered electron images of six recovered run products and the image analysis by Image J. These graphs also show the theoretical frequency curves, drawn in solid curves, with the peak being the true dihedral angle.

thermocouple junction (Supplementary Table 1 in Supporting Information S1, Figures 1c and 1d and Supplementary Figure 1 in Supporting Information S1). Melting of Fe(−Ni)−N alloy is determined by the photomicrographs (Figures 1a and 1b), indicating that (a) the isolated alloys at the interface between the silicate phases with euhedral shape rounded off the angles; and (b) most of the alloy is clustered in the triple-point junction of ringwoodite.

3.2. Phase Compositions

The chemical compositions of the alloy melt, ringwoodite, and wadsleyite in the recovered run products are reported in Supplementary Table 2 in Supporting Information S1 and plotted in Supplementary Figure 2 in Supporting Information S1. The alloy melt contained 0.88 (±0.32) wt% N for the Ni-free starting alloy mixture containing 1 wt% N, 5.5 (±0.9) to 9.7 (±0.5) wt% N and 0 to 1.5 (±0.3) wt% Ni for the one mixed with Ni-free and 4 wt% N starting mixture, and 4.1 (±0.4) to 6.0 (±1.3) wt% N and 28.4 (±5.8) to 29.3 (±2.8) wt% Ni for the starting mixture containing 4 wt% N and 10 wt% Ni. Oxygen and Si contents in the alloy melts are below 0.4 and 0.1 wt%, respectively. Ringwoodite contained 10.4 (±0.1) wt% FeO for the starting mixture with Ni−free alloy and 1 wt% N, 7.8 (±0.6) to 11.0 (±0.3) wt% FeO for the one mixed with Ni-free alloy containing 4 wt% N, and 9.6 (±0.4) to 10.6 (±0.2) wt% FeO for the one mixed with alloy containing 4 wt% N and 10 wt% Ni. Measurable NiO in ringwoodite was observed only in Exp. No. BB1669 (0.09 ± 0.03 wt%). Wadsleyite in Exp. No. BB1669 contained 7.0 (±0.6) wt% FeO and 0.06 (±0.03) wt% NiO.

3.3. Estimation of Oxygen Fugacity

Oxygen fugacity (fO_2), relative to iron-wüstite buffer (IW), is calculated from the compositions of Fe-rich alloy melt and ferropericlase following the procedure of (Mann et al., 2009):

$$\log fO_2(\mathrm{IW}) = 2\log\left[\frac{X_{FeO}^{fp}}{X_{Fe}^{alloy}}\right] + \frac{2(11{,}000 + 0.011P)\left(1 - X_{FeO}^{fp}\right)^2}{RT\ln 10} \quad (2)$$

where X_{FeO}^{fp}, X_{Fe}^{alloy}, P, and T correspond to FeO content in ferropericlase (*in* molar ratio), Fe content in alloy (*in* molar ratio), pressure in GPa, and temperature in Kelvin. X_{FeO}^{fp} can be calculated from X_{FeO}^{rw} (FeO content in ringwoodite) obtained in this study. The relation between X_{FeO}^{fp} and X_{FeO}^{rw}, which is unaffected by P and T (Frost et al., 2001), is re-fitted as;

$$X_{FeO}^{fp} = 2.311\ (\pm 0.131)\, X_{FeO}^{rw} - 1.223\ (\pm 0.178)\, (X_{FeO}^{rw})^2 \quad (3)$$

$\log fO_2$ is nearly constant versus temperature in each of the nominally Ni-free and Ni-bearing alloy melts (from IW-1.37 (±0.17) to IW-1.15 (±0.09) and from IW-0.77 (±0.04) to IW-0.64 (±0.05), respectively) (Supplementary Figure 2c in Supporting Information S1).

3.4. Dihedral Angle Between Fe(−Ni)−N Alloy and Ringwoodite

The dihedral angle distribution and theoretical frequency curve is shown in Figure 2. The deviation of the measurement is based on a 95% confidence interval around the population median (Supplementary Table 1 in Supporting Information S1 and Figure 4). Dihedral angle of nominally Ni-free alloy melt in ringwoodite, with N content in the alloy between 0.9 and 9.7 wt% and temperature varying between 1,673 and 2,073 K, ranged from $137.3^{\circ}{}^{+0.6^{\circ}}_{-3.0^{\circ}}$ to $111.9^{\circ}{}^{+0.2^{\circ}}_{-4.0^{\circ}}$. Whereas dihedral angle of Ni-bearing alloy (28.4–29.3 wt% Ni), with N content in the alloy between 4.1 and 6.0 wt% and temperature varying between 1,673 and 1,873 K alloy, ranged from $130.9^{\circ}{}^{+1.4^{\circ}}_{-4.1^{\circ}}$ to $123.9^{\circ}{}^{+2.1^{\circ}}_{-2.4^{\circ}}$.

4. Discussion

4.1. Phase Compositions and Oxygen Fugacity of the Recovered Products

The N content in the recovered alloy products tends to be higher than that in the starting materials containing 4 wt% of N in the alloy component (Supplementary Figure 2a in Supporting Information S1). This can be explained by the loss of Fe from the alloy into the MgO capsule walls during the equilibrium interaction between the constituent phases (Figure 1d). The N content in the alloy products from Ni-free starting alloy material with 4 wt% N is consistently higher than those of Ni-bearing starting alloys with the same N content at temperatures between 1,673 and 1,873 K (supplementary Figure 2a in Supporting Information S1). No systematic trends were observed for (a) FeO content in ringwoodite and (b) oxygen fugacity between Ni-free and Ni-bearing alloys (supplementary Figure 2b, 2c in Supporting Information S1). The evaluation of these trends is described in the supplementary file. We also note that the recovered alloy in the Exp. No. BB1669 contained 1.5 wt% Ni, despite the absence of Ni in the alloy starting mix, and the equilibrating ringwoodite had correspondingly lower NiO content than in the starting San Carlos olivine. Hereafter, the alloy recovered from BB1669, along with the other alloys from Ni-free starting alloy mixtures, are referred to as "nominally Ni-free alloys."

4.2. The Effects of Ni and N in Alloy Melts and Temperature on Dihedral Angle

The obtained dihedral angles of Fe(−Ni)−N alloy melts in ringwoodite is above the wetting boundary of 60° (Figure 3a), suggesting that alloy melt percolation would not occur at 20 GPa (corresponding to the condition of deep transition zone; ∼520−660 km depth). There is no significant difference in the dihedral angles between Ni-free alloy and Ni-bearing alloys (Figure 3a; BB1632 vs. BB1641 and BB1624 vs. BB1644). Because Ni content in the alloy and fO_2 are intertwined (refer to Supplementary Figure 2c; for further discussion, see Section 3 and Supplementary Figure 3 in Supporting Information S1), fO_2 does not have an apparent effect on the dihedral angle, either. At a fixed N content (BB1632 and BB1641 vs. BB1624 and BB1644), the dihedral angle decreases with increasing temperature. At a constant temperature of 1,873 K (BB1650 vs. BB1624 and BB1644), the dihedral angle decreases with increasing N content in the alloy melt. This decrease, as observed in metallurgical studies, results from the lowering of surface tension of alloy melts upon N addition. For

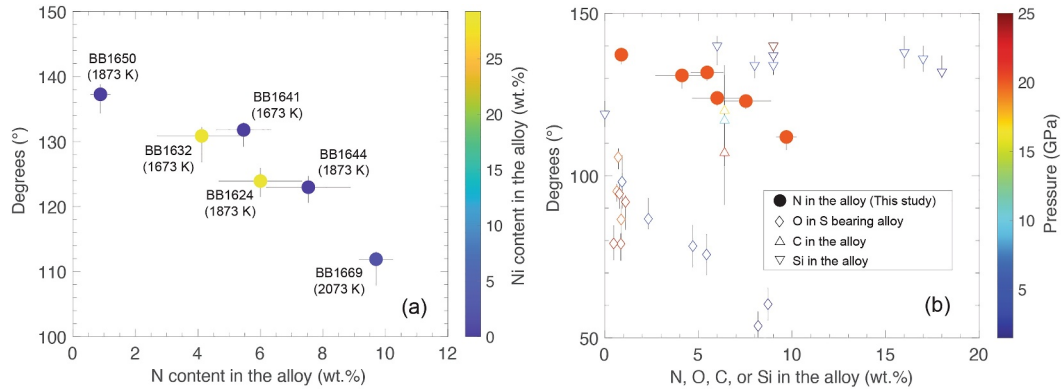

Figure 3. (a) The value of true dihedral angle in ringwoodite as a function of N content in the alloy melts on the *X*-axis, Ni content in the alloy melts by color codes, and temperature directly written on the graph. (b) The true dihedral angle in silicate minerals (olivine, wadsleyite, ringwoodite, and bridgmanite and ferropericlase mixture) as a function of the concentrations of light elements (N, O, C, and Si) on the *X*-axis and pressure (GPa) by the color codes. The data on Fe−(Ni)−N alloy melts obtained in our experiments are shown in filled circles. For comparison, the data on Fe−O−S alloy (Shannon & Agee, 1996; Terasaki et al., 2005, 2007, 2008), Fe−C alloy (Dong et al., 2019), and Fe−Si alloy (Mann et al., 2008) are also plotted in open circles, open squares, and open triangles, respectively.

example, the addition of 0.05 wt% N reduces the surface tension of the alloy melt by about 15% at 1 bar (Figure 4) (Iida & Guthrie, 2015).

4.3. Comparison With Other Light Elements in Fe(−Ni) Alloy Melts

Figure 3b shows that the dihedral angles of Fe(−Ni)−N alloys in the silicate phase (ringwoodite) at 20 GPa in this study are higher than those of Fe(−O)−S melts (Shannon & Agee, 1996; Terasaki et al., 2005, 2007, 2008; Wang & Fei, 2023) and lower than those of Fe−Si melts (Mann et al., 2008) at high pressures. This relationship is consistent with that of the surface tension of Fe−O, Fe−S, Fe−Si, and Fe−N melts under ambient pressure (Halden & Kingery, 1955; Iida & Guthrie, 2015; Kawai et al., 1974) (Figure 4). The surface tension of Fe−S and Fe−Si under high pressure (1.5 GPa) has been measured experimentally and the relative relationship is similar to the predictions at ambient pressure (Terasaki et al., 2009, 2012) (Figure 4). If the relation of the Fe−N melt surface tension remains the same as that of Fe−S and Fe−Si melts at higher pressures, the dihedral angle of Fe−Ni−N melt is expected to be larger than Fe(−O)−S melt and smaller than that of Fe−Si melt.

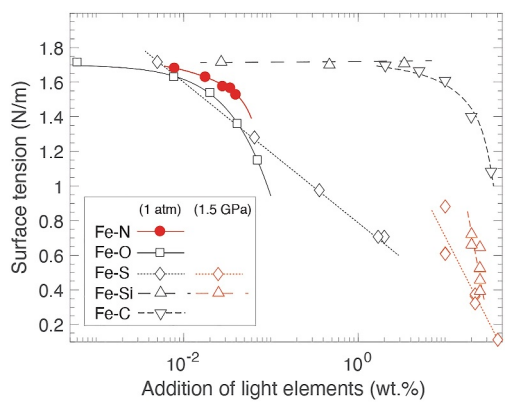

Figure 4. Surface tension of iron-rich alloy melts on aluminum oxide surface as a function of light element concentration in the alloy at ambient pressure (Halden & Kingery, 1955; Iida & Guthrie, 2015; Kawai et al., 1974) and that of Fe−S and Fe−Si melts at 1.5 GPa (Terasaki et al., 2009, 2012). Note that the absolute value of the interfacial tension may differ due to differences in the surrounding materials, for example, Na-disilicate ($Na_2Si_2O_5$) at 1.5 GPa and inert gases (H_2 or Ar) at ambient pressure, during the experiments.

On the other hand, the dihedral angle of the Fe(−Ni)−N alloy, within a similar light element concentration in the alloy, is lower than that of Fe−C alloy melts (Figure 3b) (Dong et al., 2019). These high-pressure results are in contrast to those at the ambient pressure, where the surface tension of Fe−N melt is shown to be similar to that of Fe−C melt (Figure 4).

The dihedral angle (θ) of alloy melts in solid phases (e.g., silicates such as olivine, wadsleyite, ringwoodite, and bridgmanite) is expressed as

$$2\cos\theta = \frac{\gamma_{ss}}{\gamma_{sl}} \quad (4)$$

where γ_{sl} and γ_{ss} denote solid − liquid and solid − solid interfacial energy, respectively. According to Terasaki et al. (2005), the interfacial energy can be expressed as

$$\frac{d\gamma_{sl}}{dP} \approx \Gamma_i V_i^{melt} \quad (5)$$

where Γ_i and V_i^{melt} stand for the excess concentration of component i at the surface and the partial molar volume of i in alloy melts, respectively

(i = Fe−N or Fe−C). High-pressure experiments show that iron nitrides (Fe_2N, Fe_4N, and Fe_7N_3) are more compressible than iron carbides (Fe_7C_3, Fe_3C, and Fe_2C) (Litasov et al., 2017; Zhuang et al., 2021) at elevated pressures, indicating that $\frac{d\gamma_{si}}{dP}$ for iron nitrides is more negative. Although the compressibility of Fe−N melts, unlike that of Fe−C melts (Shibazaki et al., 2015; Shimoyama et al., 2013), has not been investigated at high pressures, the difference in compressibility of iron nitrides and iron carbides indicate that the surface tension of Fe−N melts could be lower than the surface tension of Fe−C melts at high pressures. This could explain the lower dihedral angle of Fe(−Ni)−N alloy melts compared to Fe−C melts at high pressures (Figure 3b).

4.4. The Cause of N Depletion in Present-Day Bulk Silicate Earth

The extreme depletion of the N in the BSE has previously been linked to the loss of N during planetesimal differentiation (Grewal et al., 2021b, 2022a, 2022b; Grewal & Asimow, 2023), segregation of N into the Earth's core (Grewal et al., 2019a, 2021b; Jackson et al., 2021; Speelmanns et al., 2019), and loss of proto-Earth's N-bearing atmosphere(s) during impacts (Sakuraba et al., 2021; Tucker & Mukhopadhyay, 2014). Among the BSE reservoirs, the N inventory of Earth's mantle, particularly deep mantle, is poorly constrained. It is unclear whether the N depletion in the convecting mantle also reflects a deep mantle signature or if there are unsampled N-bearing reservoirs in the deep mantle. If the latter is true, N might not be as extremely depleted in the present-day BSE, especially when compared to other volatiles like carbon and water.

A recent study has shown that ferropericlase could capture a large amount of nitrogen, indicating that substantial nitrogen might be sequestered in the deep mantle after Earth's formation (Rustioni et al., 2024). Our experimental results suggest that metallic Fe, formed after the disproportionation of Fe^{2+} into Fe and Fe^{3+} at a depth >250 km, could be another potential N-bearing reservoir in the deep mantle. The dihedral angle of Fe(−Ni)−N alloy melt in a ringwoodite matrix ranged from 112° to 137°. These values are much greater than 60°, meaning interconnected networks can form only if the initial melt fraction is higher than critical melt fraction. Given the vol% of alloy initially precipitated in the deep MTZ is low (0.3−0.5 wt%); Rohrbach & Schmidt (2011), this is not feasible. If the dihedral angles of Fe(−Ni)−N alloy melt in other major mantle minerals such as olivine and bridgmanite are also similarly high, percolation of Fe(−Ni)−N alloy melt in the solid mantle remains unfeasible. Consequently, removal of excess N from the Earth's mantle via the percolation of Fe-rich alloy melt to the Earth's core cannot be a viable mechanism to explain the present-day N-depletion in the BSE. If the alloy melt was stranded in the mantle, via entrapment along grain boundaries of silicate minerals, it can instead be a hidden reservoir of N in the deep mantle. For instance, observations of iron nitride inclusions in mineral phases attest to the plausible presence of N in the Fe-rich alloys present in the deep mantle, such as Fe_3N, Fe_2N, and Fe-carbonitride (Kaminsky & Wirth, 2017). Since the estimates of the present-day N inventory of the mantle are based on natural basalts and mantle-derived volcanic gases (Marty, 1995; Marty et al., 2020; Marty & Zimmermann, 1999), they are oblivious to the presence of such a N-bearing reservoir in the non-convecting portion of Earth's mantle. The prevalence of N-bearing metallic phases in the deep mantle is currently unknown and requires further investigation.

Data Availability Statement

The raw dihedral angle data are available in an Excel file on Zenodo: Tsuno (2024).

Acknowledgments
We acknowledge the use of facilities within the Eyring Materials Center at Arizona State University supported in part by NNCI-ECCS-2025490 and the Facility for Open Research in a Compressed Environment (FORCE) at ASU supported by the National Science Foundation under Mid-scale Research Infrastructure-1 Grant 2131833. The authors thank two anonymous reviewers for their useful comments.

References

Dalou, C., Hirschmann, M. M., von der Handt, A., Mosenfelder, J., & Armstrong, L. S. (2017). Nitrogen and carbon fractionation during core–mantle differentiation at shallow depth. *Earth and Planetary Science Letters*, *458*, 141–151. https://doi.org/10.1016/j.epsl.2016.10.026

Deguen, R., Landeau, M., & Olson, P. (2014). Turbulent metal-silicate mixing, fragmentation, and equilibration in magma oceans. *Earth and Planetary Science Letters*, *391*, 274–287. https://doi.org/10.1016/j.epsl.2014.02.007

Dong, J., Li, J., & Zhu, F. (2019). Wetting behavior of iron–carbon melt in silicates at mid-mantle pressures with implications for earth's deep carbon cycle. *Frontiers in Earth Science*, *7*(October). https://doi.org/10.3389/feart.2019.00268

Frost, D., Langenhorst, F., & Van Aken, P. A. (2001). Fe-Mg partitioning between ringwoodite and magnesiowüstite and the effect of pressure, temperature and oxygen fugacity. *Physics and Chemistry of Minerals*, *28*(7), 445–470. https://doi.org/10.1007/s002690100171

Frost, D. J., & McCammon, C. A. (2008). The Redox State of earth's mantle. *Annual Review of Earth and Planetary Sciences*, *36*(1), 389–420. https://doi.org/10.1146/annurev.earth.36.031207.124322

Fukuyama, K., Kagi, H., Inoue, T., Kakizawa, S., Shinmei, T., Sano, Y., et al. (2023). Temperature dependence of nitrogen solubility in bridgmanite and evolution of nitrogen storage capacity in the lower mantle. *Scientific Reports*, *13*(1), 1–10. https://doi.org/10.1038/s41598-023-30556-5

Gaillard, F., Bouhifd, M. A., Füri, E., Malavergne, V., Marrocchi, Y., Noack, L., et al. (2021). The diverse planetary ingassing/outgassing paths produced over billions of years of magmatic activity. *Space Science Reviews*, *217*(1), 11214. https://doi.org/10.1007/s11214-021-00802-1

Genda, H., & Abe, Y. (2003). Survival of a proto-atmosphere through the stage of giant impacts: The mechanical aspects. *Icarus*, *164*(1), 149–162. https://doi.org/10.1016/S0019-1035(03)00101-5

Grewal, D. S. (2022). Origin of nitrogen isotopic variations in the rocky bodies of the solar system. *The Astrophysical Journal*, *937*(2), 123. https://doi.org/10.3847/1538-4357/ac8eb4

Grewal, D. S., & Asimow, P. D. (2023). Origin of the superchondritic carbon/nitrogen ratio of the bulk silicate earth – An outlook from iron meteorites. *Geochimica et Cosmochimica Acta*, *344*, 146–159. https://doi.org/10.1016/j.gca.2023.01.012

Grewal, D. S., Dasgupta, R., & Aithala, S. (2021c). The effect of carbon concentration on its core-mantle partitioning behavior in inner Solar System rocky bodies. *Earth and Planetary Science Letters*, *571*, 117090. https://doi.org/10.1016/j.epsl.2021.117090

Grewal, D. S., Dasgupta, R., & Farnell, A. (2020). The speciation of carbon, nitrogen, and water in magma oceans and its effect on volatile partitioning between major reservoirs of the Solar System rocky bodies. *Geochimica et Cosmochimica Acta*, *280*, 281–301. https://doi.org/10.1016/j.gca.2020.04.023

Grewal, D. S., Dasgupta, R., Holmes, A. K., Costin, G., Li, Y., & Tsuno, K. (2019b). The fate of nitrogen during core-mantle separation on Earth. *Geochimica et Cosmochimica Acta*, *251*, 87–115. https://doi.org/10.1016/j.gca.2019.02.009

Grewal, D. S., Dasgupta, R., Hough, T., & Farnell, A. (2021b). Rates of protoplanetary accretion and differentiation set nitrogen budget of rocky planets. *Nature Geoscience*, *14*(6), 369–376. https://doi.org/10.1038/s41561-021-00733-0

Grewal, D. S., Dasgupta, R., & Marty, B. (2021a). A very early origin of isotopically distinct nitrogen in inner Solar System protoplanets. *Nature Astronomy*, *5*(4), 356–364. https://doi.org/10.1038/s41550-020-01283-y

Grewal, D. S., Dasgupta, R., Sun, C., Tsuno, K., & Costin, G. (2019a). Delivery of carbon, nitrogen, and sulfur to the silicate Earth by a giant impact. *Science Advances*, *5*(1), 1–13. https://doi.org/10.1126/sciadv.aau3669

Grewal, D. S., Miyazaki, Y., & Nie, N. X. (2024). Contribution of the Moon-forming impactor to the volatile inventory in the bulk silicate Earth. *The Planetary Science Journal*, *5*(8), 181. https://doi.org/10.3847/PSJ/ad5b5d

Grewal, D. S., Seales, J. D., & Dasgupta, R. (2022a). Internal or external magma oceans in the earliest protoplanets – Perspectives from nitrogen and carbon fractionation. *Earth and Planetary Science Letters*, *598*, 117847. https://doi.org/10.1016/j.epsl.2022.117847

Grewal, D. S., Sun, T., Aithala, S., Hough, T., Dasgupta, R., Yeung, L. Y., & Schauble, E. A. (2022b). Limited nitrogen isotopic fractionation during core-mantle differentiation in rocky protoplanets and planets. *Geochimica et Cosmochimica Acta*, *338*, 347–364. https://doi.org/10.1016/j.gca.2022.10.025

Halden, F. A., & Kingery, W. D. (1955). Surface tension at elevated temperatures. II. Effect of C, N, O and S on liquid iron surface tension and interfacial energy with Al2O3. *Journal of Physical Chemistry*, *59*(6), 557–559. https://doi.org/10.1021/j150528a018

Halliday, A. N. (2013). The origins of volatiles in the terrestrial planets. *Geochimica et Cosmochimica Acta*, *105*, 146–171. https://doi.org/10.1016/j.gca.2012.11.015

Hier-Majumder, S., & Hirschmann, M. M. (2017). The origin of volatiles in the Earth's mantle. *Geochemistry, Geophysics, Geosystems*, *18*(8), 3078–3092. https://doi.org/10.1002/2017GC006937

Holness, M. B., & Lewis, S. (1997). The structure of the halite-brine interface inferred from pressure and temperature variations of equilibrium dihedral angles in the halite-H2O-CO2 system. *Geochimica et Cosmochimica Acta*, *61*(4), 795–804. https://doi.org/10.1016/S0016-7037(96)00370-5

Iida, T., & Guthrie, R. I. L. (2015). Surface tension. *The Thermophysical Properties of Metallic Liquids*, *1*, 171–218. Oxford University Press. https://doi.org/10.1093/acprof:oso/9780198729839.003.0006

Jackson, C. R. M., Cottrell, E., Du, Z., Bennett, N. R., & Fei, Y. (2021). High pressure redistribution of nitrogen and sulfur during planetary stratification. *Geochemical Perspectives Letters*, *18*, 37–42. https://doi.org/10.7185/geochemlet.2122

Kaminsky, F., & Wirth, R. (2017). Nitrides and carbonitrides from the lowermost mantle and their importance in the search for Earth's "lost" nitrogen. *American Mineralogist*, *102*(8), 1667–1676. https://doi.org/10.2138/am-2017-6101

Katsura, T. (2022). A revised adiabatic temperature profile for the mantle. *Journal of Geophysical Research: Solid Earth*, *127*(2), 1–11. https://doi.org/10.1029/2021JB023562

Katsura, T., Yoneda, A., Yamazaki, D., Yoshino, T., Ito, E., Suetsugu, D., et al. (2010). Adiabatic temperature profile in the mantle. *Physics of the Earth and Planetary Interiors*, *183*(1–2), 212–218. https://doi.org/10.1016/j.pepi.2010.07.001

Kawai, Y., Mori, K., Kishimoto, M., Ishikura, K., & Shimada, T. (1974). SURFACE TENSION OF LIQUID Fe-C-Si ALLOYS. *Tetsu-To-Hagane/Journal of the Iron and Steel Institute of Japan*, *60*(1), 29–37. https://doi.org/10.2355/tetsutohagane1955.60.1_29

Kegerreis, J. A., Teodoro, L. F. A., Eke, V. R., Massey, R. J., Catling, D. C., Fryer, C. L., et al. (2018). Consequences of giant impacts on early uranus for rotation, internal structure, debris, and atmospheric erosion. *The Astrophysical Journal*, *861*(1), 52. https://doi.org/10.3847/1538-4357/aac725

Kurokawa, H., Laneuville, M., Li, Y., Zhang, N., Fujii, Y., Sakuraba, H., et al. (2022). The origin of earth's mantle nitrogen: Primordial or early biogeochemical cycling? *Geochemistry, Geophysics, Geosystems*, *23*(5). https://doi.org/10.1029/2021GC010295

Kusakabe, M., Hirose, K., Sinmyo, R., Kuwayama, Y., Ohishi, Y., & Helffrich, G. (2019). Melting curve and equation of state of β-Fe7N3: Nitrogen in the core? *Journal of Geophysical Research: Solid Earth*, *124*(4), 3448–3457. https://doi.org/10.1029/2018JB015823

Landeau, M., Olson, P., Deguen, R., & Hirsh, B. H. (2016). Core merging and stratification following giant impact. *Nature Geoscience*, *9*(10), 786–789. https://doi.org/10.1038/ngeo2808

Leinenweber, K. D., Tyburczy, J. A., Sharp, T. G., Soignard, E., Diedrich, T., Petuskey, W. B., et al. (2012). Cell assemblies for reproducible multi-anvil experiments (the COMPRES assemblies). *American Mineralogist*, *97*(2–3), 353–368. https://doi.org/10.2138/am.2012.3844

Litasov, K. D., Shatskiy, A., Ponomarev, D. S., & Gavryushkin, P. N. (2017). Equations of state of iron nitrides ε-Fe3Nx and γ-Fe4Ny to 30 GPa and 1200 K and implication for nitrogen in the Earth's core. *Journal of Geophysical Research: Solid Earth*, *122*(5), 3574–3584. https://doi.org/10.1002/2017JB014059

Mann, U., Frost, D. J., & Rubie, D. C. (2008). The wetting ability of Si-bearing liquid Fe-alloys in a solid silicate matrix-percolation during core formation under reducing conditions? *Physics of the Earth and Planetary Interiors*, *167*(1–2), 1–7. https://doi.org/10.1016/j.pepi.2007.12.002

Mann, U., Frost, D. J., & Rubie, D. C. (2009). Evidence for high-pressure core-mantle differentiation from the metal-silicate partitioning of lithophile and weakly-siderophile elements. *Geochimica et Cosmochimica Acta*, *73*(24), 7360–7386. https://doi.org/10.1016/j.gca.2009.08.006

Marty, B. (1995). Nitrogen content of the mantle inferred from N2–Ar correlation in oceanic basalts. *Nature*, *377*(6547), 326–329. https://doi.org/10.1038/377326a0

Marty, B. (2012). The origins and concentrations of water, carbon, nitrogen and noble gases on Earth. *Earth and Planetary Science Letters*, *313–314*(1), 56–66. https://doi.org/10.1016/j.epsl.2011.10.040

Marty, B., Almayrac, M., Barry, P. H., Bekaert, D. V., Broadley, M. W., Byrne, D. J., et al. (2020). An evaluation of the C/N ratio of the mantle from natural CO2-rich gas analysis: Geochemical and cosmochemical implications. *Earth and Planetary Science Letters*, *551*, 116574. https://doi.org/10.1016/j.epsl.2020.116574

Marty, B., & Zimmermann, L. (1999). Volatiles (He, C, N, Ar) in mid-ocean ridge basalts: Assessment of shallow-level fractionation and characterization of source composition. *Geochimica et Cosmochimica Acta*, *63*(21), 3619–3633. https://doi.org/10.1016/S0016-7037(99)00169-6

Piani, L., Marrocchi, Y., Rigaudier, T., Vacher, L. G., Thomassin, D., & Marty, B. (2020). Earth's water may have been inherited from material similar to enstatite chondrite meteorites. *Science*, *369*(6507), 1110–1113. https://doi.org/10.1126/science.aba1948

Rohrbach, A., Ballhaus, C., Golla-Schindler, U., Ulmer, P., Kamenetsky, V. S., & Kuzmin, D. V. (2007). Metal saturation in the upper mantle. *Nature*, *449*(7161), 456–458. https://doi.org/10.1038/nature06183

Rohrbach, A., & Schmidt, M. W. (2011). Redox freezing and melting in the Earths deep mantle resulting from carbon-iron redox coupling. *Nature*, *472*(7342), 209–214. https://doi.org/10.1038/nature09899

Rudge, J. F., Kleine, T., & Bourdon, B. (2010). Broad bounds on Earths accretion and core formation constrained by geochemical models. *Nature Geoscience*, *3*(6), 439–443. https://doi.org/10.1038/ngeo872

Rustioni, G., Wiedenbeck, M., Miyajima, N., Chanyshev, A., & Keppler, H. (2024). Magnesiowüstite as a major nitrogen reservoir in Earth´s lowermost mantle. *Geochemical Perspectives Letters*, *28*, 43–47. https://doi.org/10.7185/geochemlet.2401

Sakuraba, H., Kurokawa, H., Genda, H., & Ohta, K. (2021). Numerous chondritic impactors and oxidized magma ocean set Earth's volatile depletion. *Scientific Reports*, *11*(1), 1–14. https://doi.org/10.1038/s41598-021-99240-w

Schlichting, H. E., Sari, R., & Yalinewich, A. (2015). Atmospheric mass loss during planet formation: The importance of planetesimal impacts. *Icarus*, *247*, 81–94. https://doi.org/10.1016/j.icarus.2014.09.053

Shannon, M. C., & Agee, C. B. (1996). High pressure constraints on percolative core formation. *Geophysical Research Letters*, *23*(20), 2717–2720. https://doi.org/10.1029/96GL02817

Shibazaki, Y., Kono, Y., & Fei, Y. (2015). Microscopic structural change in a liquid Fe-C alloy of ∼5GPa. *Geophysical Research Letters*, *42*(13), 5236–5242. https://doi.org/10.1002/2015GL064271

Shimoyama, Y., Terasaki, H., Ohtani, E., Urakawa, S., Takubo, Y., Nishida, K., et al. (2013). Density of Fe-3.5wt% C liquid at high pressure and temperature and the effect of carbon on the density of the molten iron. *Physics of the Earth and Planetary Interiors*, *224*, 77–82. https://doi.org/10.1016/j.pepi.2013.08.003

Speelmanns, I. M., Schmidt, M. W., & Liebske, C. (2019). The almost lithophile character of nitrogen during core formation. *Earth and Planetary Science Letters*, *510*, 186–197. https://doi.org/10.1016/j.epsl.2019.01.004

Suer, T.-A., Jackson, C., Grewal, D. S., Dalou, C., & Lichtenberg, T. (2023). The distribution of volatile elements during rocky planet formation. *Frontiers in Earth Science*, *11*. https://doi.org/10.3389/feart.2023.1159412

Terasaki, H., Frost, D. J., Rubie, D. C., & Langenhorst, F. (2005). The effect of oxygen and sulphur on the dihedral angle between Fe-O-S melt and silicate minerals at high pressure: Implications for Martian core formation. *Earth and Planetary Science Letters*, *232*(3–4), 379–392. https://doi.org/10.1016/j.epsl.2005.01.030

Terasaki, H., Frost, D. J., Rubie, D. C., & Langenhorst, F. (2007). Interconnectivity of Fe-O-S liquid in polycrystalline silicate perovskite at lower mantle conditions. *Physics of the Earth and Planetary Interiors*, *161*(3–4), 170–176. https://doi.org/10.1016/j.pepi.2007.01.011

Terasaki, H., Frost, D. J., Rubie, D. C., & Langenhorst, F. (2008). Percolative core formation in planetesimals. *Earth and Planetary Science Letters*, *273*(1–2), 132–137. https://doi.org/10.1016/j.epsl.2008.06.019

Terasaki, H., Urakawa, S., Funakoshi, K., Nishiyama, N., Wang, Y., Nishida, K., et al. (2009). In situ measurement of interfacial tension of Fe-S and Fe-P liquids under high pressure using X-ray radiography and tomography techniques. *Physics of the Earth and Planetary Interiors*, *174*(1–4), 220–226. https://doi.org/10.1016/j.pepi.2009.01.004

Terasaki, H., Urakawa, S., Rubie, D. C., Funakoshi, K., Sakamaki, T., Shibazaki, Y., et al. (2012). Interfacial tension of Fe-Si liquid at high pressure: Implications for liquid Fe-alloy droplet size in magma oceans. *Physics of the Earth and Planetary Interiors*, *202–203*, 1–6. https://doi.org/10.1016/j.pepi.2012.05.002

Tsuno, K. (2024). Raw dihedral angle data_Tsuno et al. (2024) GRL. [Dataset]. https://doi.org/10.5281/zenodo.13362485. *Zenodo*.

Tsuno, K., Grewal, D. S., & Dasgupta, R. (2018). Core-mantle fractionation of carbon in Earth and Mars: The effects of sulfur. *Geochimica et Cosmochimica Acta*, *238*, 477–495. https://doi.org/10.1016/j.gca.2018.07.010

Tucker, J. M., & Mukhopadhyay, S. (2014). Evidence for multiple magma ocean outgassing and atmospheric loss episodes from mantle noble gases. *Earth and Planetary Science Letters*, *393*, 254–265. https://doi.org/10.1016/j.epsl.2014.02.050

von Bargen, N., & Waff, H. S. (1986). Permeabilities, interfacial areas and curvatures of partially molten systems: Results of numerical computations of equilibrium microstructures. *Journal of Geophysical Research*, *91*(B9), 9261–9276. https://doi.org/10.1029/jb091ib09p09261

Wang, L., & Fei, Y. (2023). A partially equilibrated initial mantle and core indicated by stress-induced percolative core formation through a bridgmanite matrix. *Science Advances*, *9*(7), 1–9. https://doi.org/10.1126/sciadv.ade3010

Woodland, A. B., & Koch, M. (2003). Variation in oxygen fugacity with depth in the upper mantle beneath the Kaapvaal craton, Southern Africa. *Earth and Planetary Science Letters*, *214*(1–2), 295–310. https://doi.org/10.1016/S0012-821X(03)00379-0

Yoshioka, T., Wiedenbeck, M., Shcheka, S., & Keppler, H. (2018). Nitrogen solubility in the deep mantle and the origin of Earth's primordial nitrogen budget. *Earth and Planetary Science Letters*, *488*, 134–143. https://doi.org/10.1016/j.epsl.2018.02.021

Zahnle, K., Arndt, N., Cockell, C., Halliday, A., Nisbet, E., Selsis, F., & Sleep, N. H. (2007). Emergence of a habitable planet. *Space Science Reviews*, *129*(1–3), 35–78. https://doi.org/10.1007/s11214-007-9225-z

Zedgenizov, D. A., & Litasov, K. D. (2017). Looking for "missing" nitrogen in the deep Earth. *American Mineralogist*, *102*(9), 1769–1770. https://doi.org/10.2138/am-2017-6218

Zhuang, Y., Su, X., Salke, N. P., Cui, Z., Hu, Q., Zhang, D., & Liu, J. (2021). The effect of nitrogen on the compressibility and conductivity of iron at high pressure. *Geoscience Frontiers*, *12*(2), 983–989. https://doi.org/10.1016/j.gsf.2020.04.012